Available online at www.sciencedirect.com
ScienceDirect
Trans. Nonferrous Met. Soc. China 33(2023) 3756−3769
Transactions of Nonferrous Metals Society of China
www.tnmsc.cn

Effects of Sc addition on microstructure, phase evolution and mechanical properties of $Al_{0.2}CoCrFeNi$ high-entropy alloys

Yuan-wei SUN[1], Zi-yi WANG[1], Xiang-jin ZHAO[1], Zhong-li LIU[1], Fu-hua CAO[2]

1. School of Nuclear Equipment and Nuclear Engineering, Yantai University, Yantai 264005, China;
2. Institute of Mechanics, Chinese Academy of Sciences, Beijing 100190, China

Received 4 January 2023; accepted 10 August 2023

Abstract: $Al_{0.2}CoCrFeNiSc_x$ (x=0, 0.1, 0.2 and 0.3, molar fraction) alloys were prepared by arc melting. The effects of Sc addition on the microstructure, phase evolution and mechanical properties of $Al_{0.2}CoCrFeNiSc_x$ alloys were investigated. The results showed that Sc could refine grain size, change phase type and improve mechanical properties. The grain size of $Al_{0.2}CoCrFeNiSc_{0.3}$ alloy (8.5 μm) was reduced by approximately 50.6% compared to that of $Al_{0.2}CoCrFeNiSc_{0.1}$ alloy (17.2 μm). The crystal structure evolved from a single FCC phase to a mixed phase including two types of FCC phases and one type of BCC phase. The FCC phase mainly appeared in the regions of (Co, Cr, Fe)-rich dendrites and (Ni, Sc)-rich interdendrites; while the BCC phase was mainly located in the region of (Al, Ni)-rich interdendrites. The yield strength increased from 167 to 717 MPa as the x value in $Al_{0.2}CoCrFeNiSc_x$ alloy increased from 0 to 0.3, improved by 329.3%, which could be attributed to grain size strengthening, solid solution strengthening and phase evolution.

Key words: high-entropy alloy; phase evolution; microstructure; grain refinement; yield strength

1 Introduction

High-entropy alloys (HEAs) exhibit high mechanical strength and/or ductility [1], superior compressive or extensive properties [2], high hardness [3], excellent impact toughness [4], special electrical and magnetic properties [5], and good catalytic performance [6], which makes them potential candidates for engineering applications. To date, many HEA systems have been exploited, e.g., $Al_xCoCrFeNi$ [7,8], CoCrFe(Mn, Cu, Nb)-Ni [9,10], AlCoCuFeNi [11], and AlCoCrFeNi-(Cu, Mn, Si, Ti, V) [12−14]. In particular, $Al_xCoCrFeNi$ has been comprehensively researched because it combines high compressive strength and hardness, excellent fracture toughness and work hardenability coupled with low cost and abundant constituent elements.

The effects of alloying elements, such as Al, Cu, Ti, V, Nb, Y, B, and Si, on the structure and properties of AlCoCrFeNi alloys have attracted extensive attention from researchers. Adding Al to an $Al_xCoCrFeNi$ alloy changes the crystal structure [15]. Specifically, the $Al_xCoCrFeNi$ alloy transforms from a single FCC structure to an FCC+BCC structure and finally to a single BCC structure for $0\leq x<0.5$, $0.5\leq x<0.9$ and $0.9\leq x<3.0$, respectively. Changes in the crystal structure consequently vary the material properties [16]. Adding Cu to the as-cast AlCoCrFeNi could improve the wear resistance, but it decreased the corrosion resistance of the alloy [17]. The addition of Ti [18], V [19] and Y [20] to HEA alloys could improve the mechanical properties due to the formation of BCC structure and new phase. The addition of Nb and Si could modify the phase compositions and properties of the AlCoCrFeNi

Corresponding author: Yuan-wei SUN, Tel: +86-17861100926, E-mail: sunywytu@163.com;
Xiang-jin ZHAO, Tel: +86-15953572863, E-mail: zhaoxjworld@163.com
DOI: 10.1016/S1003-6326(23)66368-X

alloys [21,22]. The addition of B improved the hardness and wear resistance of the $Al_{0.5}CoCrCuFeNi$ alloy but decreased the toughness [23].

Sc is located in the IIIB group and the fourth period of the periodic table, the same period as Ti, V, Cr, Fe, Co, and Ni. It is usually added to aluminium alloys, e.g., 2××× series, 5××× series, 7××× series, Al−Mg−Li and Al−Li−Cu−Mg alloys, as a microalloying element to refine the grain [24,25], improve the mechanical properties [26], corrosion resistance [27−29] and welding performance [30]. The improvement in these properties is due to the formation of coherent Al_3Sc nanoparticles with $L1_2$ structure, which significantly affect the grain refinement, precipitation strengthening and recrystallization inhibition [31]. In addition to effectively improving the properties of aluminium alloy, the addition of Sc can improve the mechanical properties of TiAl alloy [32,33], creep resistance of magnesium alloy [34], and mechanical properties of steels [35]. The effect of Sc addition to HEA alloys has been investigated recently. Alloying 0.3−0.5 wt.% Sc addition to the $Al_2CoCrFeNi$, $Al_{0.5}CoCrCuFeNi$ and $AlCoCrCu_{0.5}FeNi$ causes the grain refinement, and the increase of the hardness and electrical conductivity [36]. In addition, adding 3 wt.% Sc to $Al_2CoCrFeNi$ alloy leads to the precipitation of Al_2Cu_3Sc intermetallic, which has significantly improved the hardness and thermal stability of the alloy [37]. Sc has also been incorporated as one of the principal elements into AlCrCuScTi [38], $Al_{20}Li_{20}Mg_{10}Sc_{20}Ti_{30}$ [39], CoGdYScTiZr [40], ScYLaTiZrHf [41], and ScHfNbTaTiZr [42] alloys. Sc is not only used as a trace element but also as a major alloying element, for Al alloys first and increasingly now to HEA alloys. It is clear that more fundamental research is required to extend the investigation about the influence of Sc on the microstructure and properties of HEA alloys.

In the present study, a series of $Al_{0.2}CoCrFeNiSc_x$ (x=0, 0.1, 0.2, 0.3, molar fraction) alloys were prepared using arc melting method. The purpose of this work was to investigate the effects of Sc addition on the microstructure, phase evolution and mechanical properties of the studied alloys. This work will be of great significance for enriching the composition design of HEA alloys and further providing a new perspective for exploring the potential properties of HEA alloys.

2 Experimental

Ingots with nominal $Al_{0.2}CoCrFeNiSc_x$ compositions were prepared by arc melting in an argon atmosphere. The purities of the metal particles were 99.9% for Al, 99.95% for Co, 99.99% for Cr, 99.99% for Fe, 99.995% for Ni and 99.99% for Sc. The ingot was remelted at least four times to ensure chemical homogeneity, and all samples were tested under as-cast conditions. Table 1 shows the measured chemical compositions of the nominal $Al_{0.2}CoCrFeNiSc_x$ alloys using the SPECTRO BLUE SOP ICP test. The measured composition of each ingot is close to its nominal composition.

X-ray diffraction (XRD), metallographic microscopy (OM), scanning electron microscopy (SEM), electron back-scattered diffraction (EBSD) and scanning transmission electron microscopy (STEM) were chosen to observe and analyze the microstructure. The specimens for XRD, OM and SEM observation were prepared by mechanical polishing. The polished faces were etched in a mixed solution of 75 vol.% HCl and 25 vol.%

Table 1 Measured chemical compositions of nominal $Al_{0.2}CoCrFeNiSc_x$ alloys

Alloy	Composition	Content/wt.%					
		Al	Co	Cr	Fe	Ni	Sc
$Al_{0.2}CoCrFeNi$	Nominal	2.34	25.53	22.52	24.19	25.42	
	Measured	2.41	25.7	22.7	23.5	25.4	
$Al_{0.2}CoCrFeNiSc_{0.1}$	Nominal	2.29	25.04	22.09	23.73	24.94	1.91
	Measured	2.36	25.3	22.3	23.5	24.6	1.81
$Al_{0.2}CoCrFeNiSc_{0.2}$	Nominal	2.25	24.57	21.68	23.28	24.47	3.75
	Measured	2.39	24.4	21.8	23.3	24.2	3.71
$Al_{0.2}CoCrFeNiSc_{0.3}$	Nominal	2.21	24.12	21.28	22.86	24.02	5.52
	Measured	2.32	24.3	21.5	22.1	24.1	5.63

HNO_3 for OM and SEM observation. XRD data were collected on a Bruker D8 Advance diffractometer with Cu K_{α_1} radiation in the 2θ range from 10° to 80° with a scanning rate of 2 (°)/min to identify the crystal structure of the alloy. OM images were taken using an Axio Observer microscope. A JSM−7610F microscope was used to observe the microstructure, and energy dispersive X-ray spectroscopy (EDS) was used to detect the chemical composition. The Oxford Symmetry EBSD detector was used to detect the crystal structure. STEM investigations were carried out on a Talos F200X G2 microscope at 200 kV to observe the microstructure and analyze the chemical composition. The specimens for the TEM measurements were prepared using a Fischione 1051 ion thinning instrument.

Hardness tests were performed on an HV−1000A type digital Vickers micro-sclerometer under a load of 500 g for 10 s. The mean value of at least six measurements was taken as the final value. Compression samples with a diameter of 4 mm and a height of 6 mm were cut from the as-cast ingot. A UTM5105X electronic universal testing machine was used for compression tests at a constant rate of 0.5 mm/min. Three tests were needed for the sample for each composition.

3 Results

3.1 Microstructure and phase evolution

Figure 1 shows the X-ray diffraction patterns of $Al_{0.2}CoCrFeNiSc_x$ alloys. For the $Al_{0.2}CoCrFeNi$ alloy, only FCC diffraction peaks were observed, which indicated that the crystal structure of the $Al_{0.2}CoCrFeNi$ alloy was a single FCC. When Sc was added to the $Al_{0.2}CoCrFeNi$ alloy, another set of FCC diffraction peaks and BCC diffraction peaks appeared, as clearly seen in Fig. 1(b). This finding implies that the crystal structure of $Al_{0.2}CoCrFeNiSc_x$ alloys evolves from a single FCC structure for x=0 to a mixed FCC+BCC structure for x=0.1, 0.2, 0.3. The addition of Sc modified the crystal structure of $Al_{0.2}CoCrFeNiSc_x$ alloys, which will have an important effect on the mechanical properties.

Figure 2 shows the metallographic structure of $Al_{0.2}CoCrFeNiSc_x$ alloys. As shown in Fig. 2(a), the $Al_{0.2}CoCrFeNi$ alloy exhibited a wicker-shaped morphology, and the wicker-shaped trunks grew parallel and closely along a specific crystal orientation. The microstructure displayed a columnar dendritic structure after the addition of Sc to $Al_{0.2}CoCrFeNi$ alloys. With increasing Sc content, the number of dendrites increased, whereas the arm width and length decreased. Accordingly, the arm width and length of the interdendrite increased, which indicated that the negative mixing enthalpy and the large difference in atomic size caused component supercooling due to the Sc addition [43]. The dendritic and interdendritic regions consisted of alternating bright and dark phases. Each columnar dendritic and interdendritic structure grew along a specific crystal orientation. In the $Al_{0.2}CoCrFeNiSc_{0.1}$ alloy, the arm widths of the primary and secondary dendrites were large (marked by red arrows in Fig. 2(b)), approximately 18 and 10 μm, respectively. As the content of Sc increased to 0.2, the arm widths of the primary and secondary dendrites decreased (Fig. 2(c)). When the

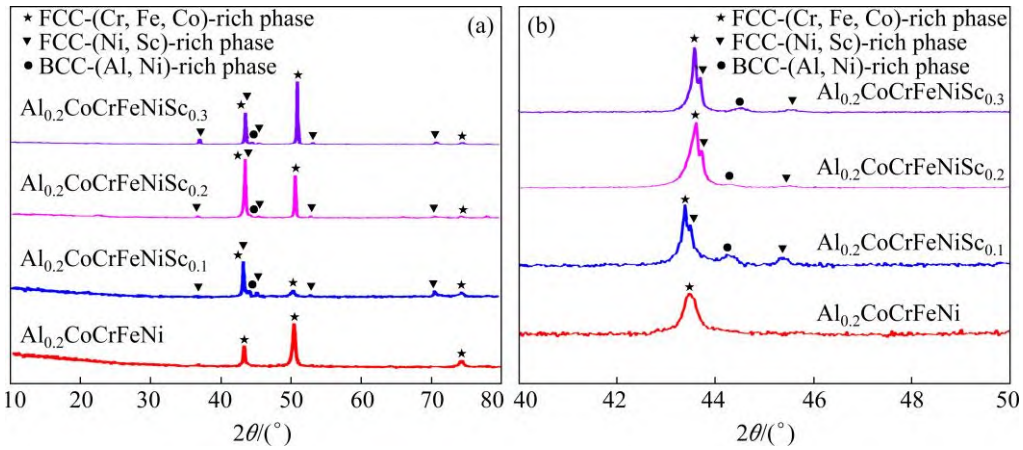

Fig. 1 XRD patterns of $Al_{0.2}CoCrFeNiSc_x$ alloys with different Sc contents: (a) XRD patterns in 2θ range of 10°−80°; (b) Enlarged view of XRD patterns in 2θ range of 40°−50°

content of Sc increased to 0.3, almost no primary dendrites were observed, and some secondary dendrites were transformed into near-equiaxed grains, as shown in Fig. 2(d). This finding implied that the addition of Sc had a grain-refining effect on the studied alloy.

The grain sizes of the $Al_{0.2}CoCrFeNiSc_{0.1}$, $Al_{0.2}CoCrFeNiSc_{0.2}$ and $Al_{0.2}CoCrFeNiSc_{0.3}$ alloys were obtained with the Image Pro-Plus software based on the OM images to better clarify the refining effect of Sc. During the calculation, the secondary dendrite arm spacing was used for measuring the grain size [24,44]. As listed in Table 2, the grain sizes of the $Al_{0.2}CoCrFeNiSc_{0.1}$, $Al_{0.2}CoCrFeNiSc_{0.2}$ and $Al_{0.2}CoCrFeNiSc_{0.3}$ alloys were 17.2, 10.2 and 8.5 μm, respectively. As the Sc content increased, the grain size decreased. The grain size of $Al_{0.2}CoCrFeNiSc_{0.3}$ alloy was reduced by approximately 50.6% compared to that of $Al_{0.2}CoCrFeNiSc_{0.1}$ alloy.

Figure 3 shows SEM images of $Al_{0.2}CoCrFeNiSc_x$ alloys. The $Al_{0.2}CoCrFeNi$ alloy with a single FCC structure had a columnar cellular microstructure (see Fig. 3(a)). The $Al_{0.2}CoCrFeNiSc_{0.1}$, $Al_{0.2}CoCrFeNiSc_{0.2}$ and $Al_{0.2}CoCrFeNiSc_{0.3}$ alloys consisted of dendritic and interdendritic microstructures (Figs. 3(b−d)). The interdendritic regions *B* and *C* in Fig. 3(b), i.e., grey interdendritic regions and black interdendritic regions, had different morphologies. The black interdendrite exhibited a stripe shape (see the enlarged view in Fig. 3(b)). EDS measurement was performed to test the chemical compositions of dendrites and interdendrites, and the results are shown in Fig. 4. Specifically, the dendritic region was a (Co, Cr, Fe)-rich phase (Position *A* in Fig. 4(a)), and the grey-coloured interdendritic region was a (Ni, Sc)-rich phase (Position *B* in Fig. 4(a)).

The stripe-shaped interdendritic region was an (Al, Ni)-rich phase (marked by Position *C* in Fig. 4(a)). In addition, Sc was mainly distributed in the interdendritic region, especially the grey interdendritic region *B* in Fig. 4(a). As the Sc content increased, the (Co, Cr, Fe)-rich phases decreased, and the (Ni, Sc)-rich and (Al, Ni)-rich phases increased.

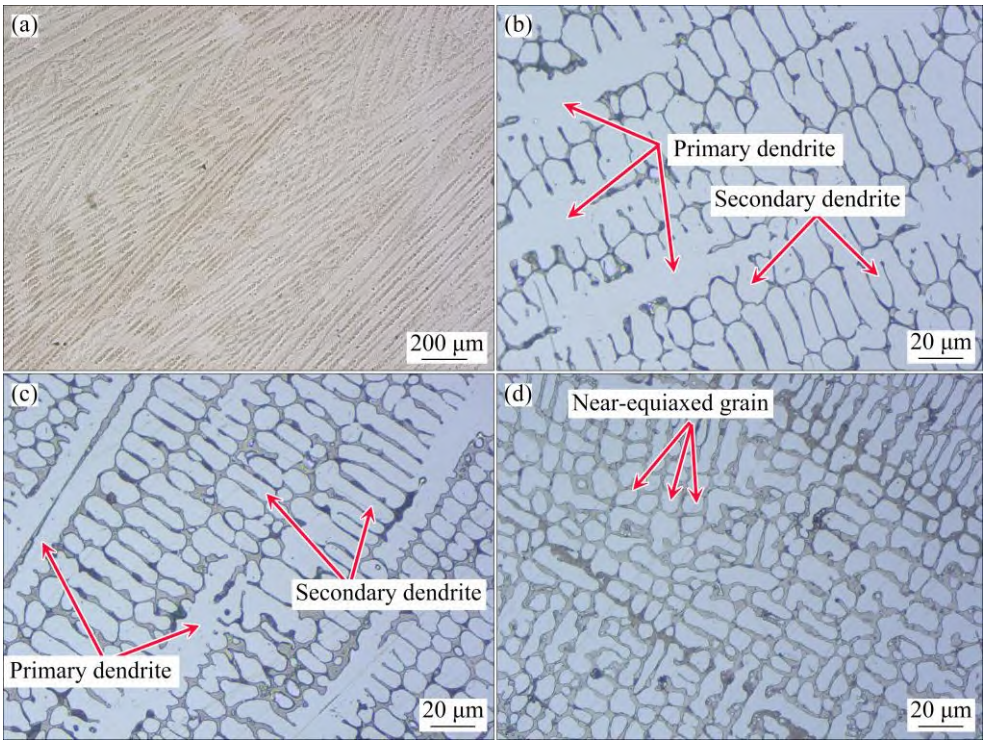

Fig. 2 Metallographic structures of $Al_{0.2}CoCrFeNiSc_x$ alloys: (a) x=0; (b) x=0.1; (c) x=0.2; (d) x=0.3

Table 2 Grain sizes of $Al_{0.2}CoCrFeNiSc_x$ alloys

Alloy	$Al_{0.2}CoCrFeNiSc_{0.1}$	$Al_{0.2}CoCrFeNiSc_{0.2}$	$Al_{0.2}CoCrFeNiSc_{0.3}$
Grain size/μm	17.2	10.2	8.5

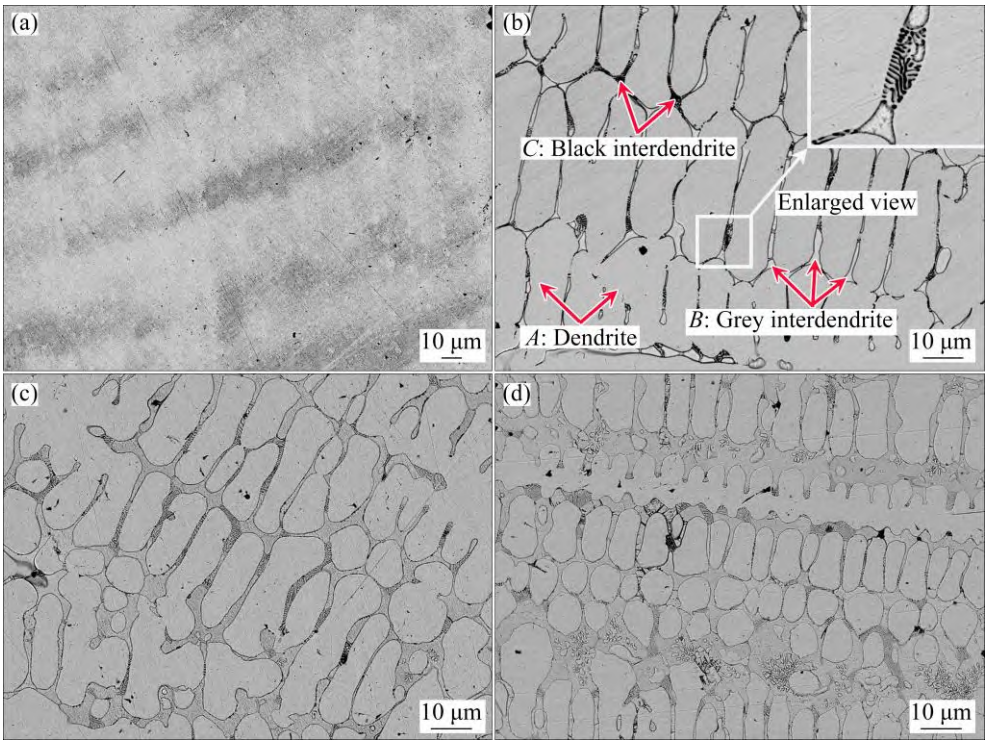

Fig. 3 SEM images of $Al_{0.2}CoCrFeNiSc_x$ alloys: (a) x=0; (b) x=0.1; (c) x=0.2; (d) x=0.3

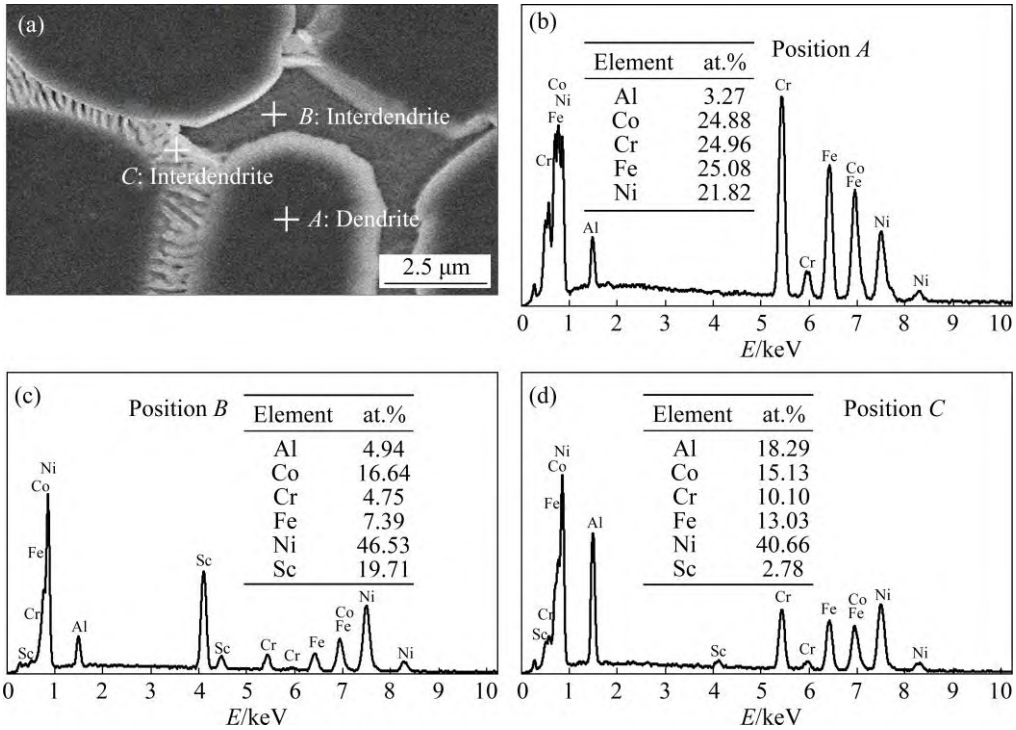

Fig. 4 EDS data of different regions in Fig. 3(b)

Figure 5 shows the EBSD phase map of $Al_{0.2}CoCrFeNiSc_{0.1}$ alloy. The columnar dendritic structure mainly consisted of FCC and BCC phases. The FCC phase appeared in the regions of (Co, Cr, Fe)-rich dendrites and (Ni, Sc)-rich interdendrites. The BCC phase was primarily located in the (Al, Ni)-rich interdendritic region with stripe shape.

Figure 6 shows the TEM images and the corresponding diffraction patterns (DPs) of the $Al_{0.2}CoCrFeNi$ and $Al_{0.2}CoCrFeNiSc_{0.1}$ alloys. For

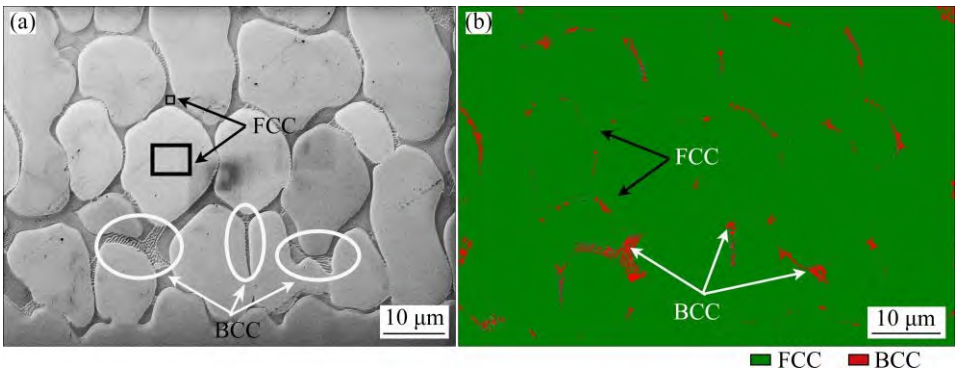

Fig. 5 EBSD images showing distribution of FCC and BCC phases for $Al_{0.2}CoCrFeNiSc_{0.1}$ alloy: (a) EBSD band contrast; (b) Phase distribution image

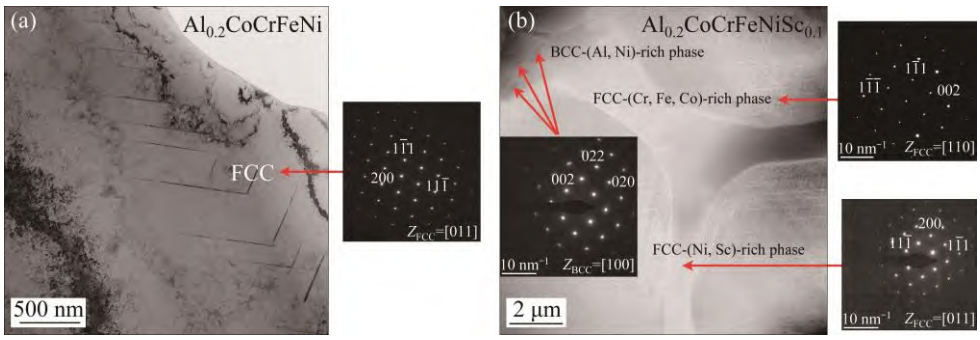

Fig. 6 TEM images and corresponding diffraction patterns of $Al_{0.2}CoCrFeNi$ (a) and $Al_{0.2}CoCrFeNiSc_{0.1}$ (b) alloys

the $Al_{0.2}CoCrFeNi$ alloy, the DP in Fig. 6(a) demonstrated that only FCC phase existed in the alloy, which is in accordance with the XRD results shown in Fig. 1(a). For the $Al_{0.2}CoCrFeNiSc_{0.1}$ alloy, as shown in Fig. 6(b), the (Co, Cr, Fe)-rich dendritic phase and (Ni, Sc)-rich interdendritic phase were confirmed to be FCC structure, while the (Al, Ni)-rich interdendritic phase was confirmed to be BCC structure. This result was in good agreement with the EBSD result shown in Fig. 5. It was reported that Ni_2Sc has a $MgCu_2$-type FCC structure and can be formed by the following reactions: Liquid $\rightleftharpoons$ Ni_7Sc_2 + Ni_2Sc at 1270 °C, Liquid$\rightleftharpoons$$Ni_2Sc$ at 1330 °C and Liquid$\rightleftharpoons$$Ni_2Sc$ + NiSc at 1100 °C [45]. In addition, Ni_2Sc formed a homogeneous solid solution in the range of 27−35 at.% Sc [46]. As shown in Fig. 4(c), the molar fraction of Ni and Sc was 46.53% and 19.71%, respectively, which was close to that of Ni_2Sc. Besides, the (Ni, Sc)-rich phase was confirmed to be FCC structure by EBSD and TEM, which was the same as the Ni_2Sc phase structure. In summary, the chemical formula of (Ni, Sc)-rich phase was possibly Ni_2Sc.

STEM mapping was performed to further analyze the element distributions of $Al_{0.2}CoCrFeNi$ and $Al_{0.2}CoCrFeNiSc_{0.1}$ alloys, and the results are shown in Fig. 7 and Fig. 8, respectively. Figure 7 indicated that element segregation did not occur in the entire tested region for the $Al_{0.2}CoCrFeNi$ alloy. However, when Sc was added to the $Al_{0.2}CoCrFeNi$ alloy, an apparent segregation phenomenon appeared, as shown in Fig. 8. Co, Cr and Fe were more concentrated in the dendritic region, marked by the circle in Fig. 8. Ni and Sc were primarily segregated into the interdendritic region with an FCC structure, marked by the triangle in Fig. 8. Al and Ni were mainly segregated into the interdendritic region with a BCC structure, marked by the rectangle in Fig. 8. This result agreed with that reported by WANG et al [15]. For the $Al_xCoCrFeNi$ alloy with $x \geq 0.7$, the FCC structure was an (Fe, Cr)-rich phase, and the BCC structure was an (Al, Ni)-rich phase. Figure 8 also shows that a small amount of Sc remained segregated in the interdendritic region with a BCC structure, although the majority segregated into the interdendritic region with an FCC structure.

3.2 Hardness and compressive property

Figure 9 shows the hardness of $Al_{0.2}CoCrFeNiSc_x$ alloys. For the $Al_{0.2}CoCrFeNi$ alloy with a single

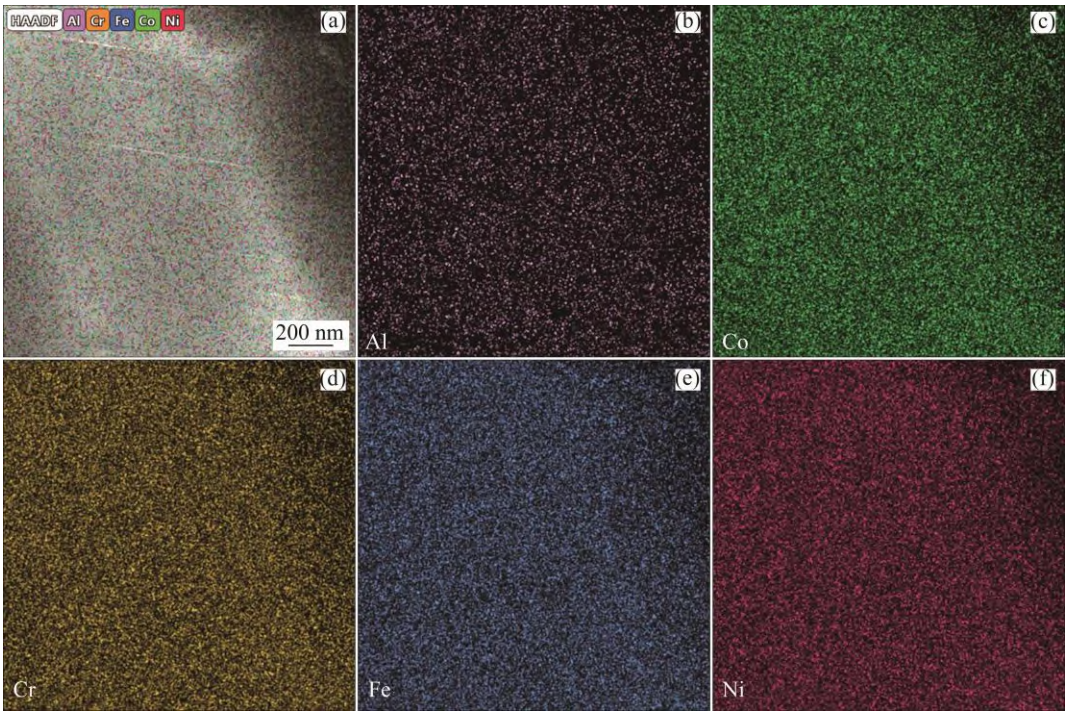

Fig. 7 STEM image of $Al_{0.2}CoCrFeNi$ alloy with corresponding element distribution mappings: (a) TEM image; (b) Al; (c) Co; (d) Cr; (e) Fe; (f) Ni

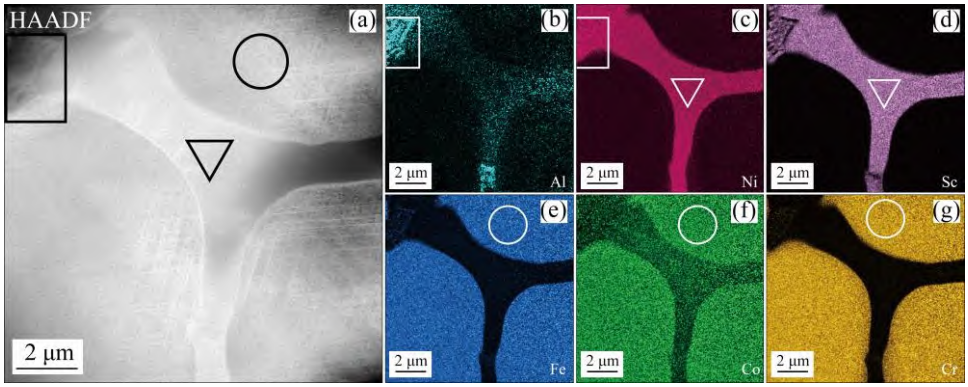

Fig. 8 STEM image of $Al_{0.2}CoCrFeNiSc_{0.1}$ alloy with corresponding element distribution mappings: (a) TEM image; (b) Al; (c) Ni; (d) Sc; (e) Fe; (f) Co; (g) Cr

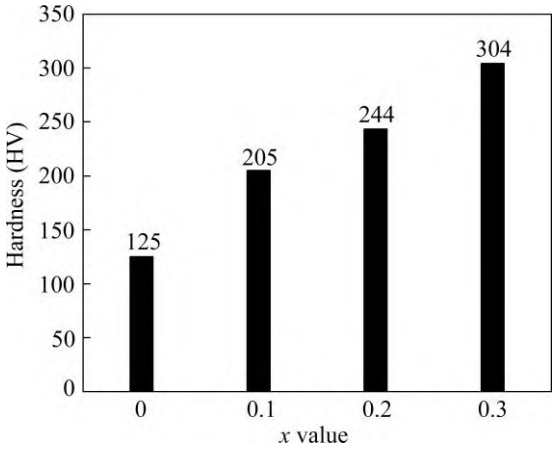

Fig. 9 Hardness of $Al_{0.2}CoCrFeNiSc_x$ alloys

FCC structure, the hardness was only HV 125. However, the hardness dramatically increased after the addition of Sc. For the $Al_{0.2}CoCrFeNiSc_{0.3}$ alloy, the hardness reached HV 304, an improvement of 143.2% compared to that of $Al_{0.2}CoCrFeNi$ alloy.

The mechanical properties of $Al_{0.2}CoCrFeNiSc_x$ alloys were evaluated by compression tests, and the results are shown in Fig. 10. Notably, the yield strength and ductility strongly depended on the Sc content. The $Al_{0.2}CoCrFeNi$, $Al_{0.2}CoCrFeNiSc_{0.1}$ and $Al_{0.2}CoCrFeNiSc_{0.2}$ alloys externally appeared intact. The side surfaces appeared to be cracked but not crushed after the compression test (see the

insert in Fig. 10(a)). This morphology corresponded to a high strain value, indicating excellent ductility. However, the $Al_{0.2}CoCrFeNiSc_{0.3}$ alloy was crushed after the compression test, corresponding to a lower strain value of only 28.6%. In contrast to the ductility, the yield strength increased as the Sc content increased. The yield strength increased almost linearly from 167 to 717 MPa as x increased from 0 to 0.3, as shown in Fig. 10(b), which indicated that adding Sc to the $Al_{0.2}CoCrFeNi$ alloy improved its strength.

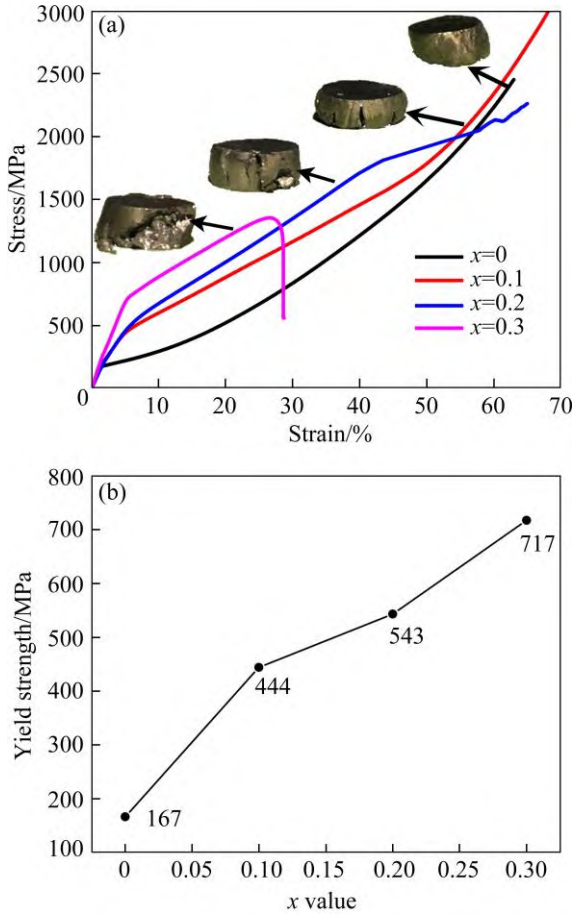

Fig. 10 Compressive stress−strain curves of $Al_{0.2}CoCrFeNiSc_x$ alloys (a) and yield strength as function of x value (b)

4 Discussion

4.1 Effect of Sc on microstructure and phase evolution

As the Sc content increased from 0.1 to 0.3, the grain size of the alloy decreased from 17.2 to 8.5 μm, as shown in Table 2, which implied that Sc had the grain-refining effect. The element segregation in the front of the solid−liquid interface decreased as the Sc content increased and the constitutional supercooling decreased, thereby inhibiting the extension of the primary dendrite and the growth of the secondary dendrite. As a result, the grain size decreased. Sc is generally believed to act as a powerful grain refiner in aluminium alloys, which effectively refines the structure. MOUSAVI et al [47] reported that the grain size of casting 7108 aluminium alloy decreased from 380 to 50 μm after adding 0.3 wt.% Sc to the alloy. In addition, a powerful grain-refining effect occurred in the casting 7050 aluminium alloy: when the Sc content reached 0.28 wt.%, the grain size decreased from 250 to 60 μm [48]. In the present study, adding Sc to the $Al_{0.2}CoCrFeNi$ alloy also had a grain-refining effect, which will greatly influence the mechanical properties of the alloy.

Previous studies have reported that $Al_xCoCrFeNi$ alloys had a single FCC structure for $x < 0.4$ [16,49,50], while they evolved into a mixed FCC and BCC structure for $0.4 < x < 0.9$ [15,51]. When Sc was added to the alloy, the structure changed from a single FCC phase ($Al_{0.2}CoCrFeNi$ alloy) to a mixed phase ($Al_{0.2}CoCrFeNiSc_{0.1}$, $Al_{0.2}CoCrFeNiSc_{0.2}$ and $Al_{0.2}CoCrFeNiSc_{0.3}$ alloys), including two types of FCC phases and one type of BCC phase based on the analysis of XRD patterns (Fig. 1), SEM images (Fig. 3), EBSD images (Fig. 5) and TEM images (Fig. 6). Table 3 lists the mixing enthalpies of atom pairs between each element. The mixing enthalpy between Sc and Ni was the most negative, −39 kJ/mol, which could be the reason for the formation of the (Ni, Sc)-rich phase with an FCC structure. The mixing enthalpy between Al and Ni was also relatively negative, −22 kJ/mol. This finding indicated that Al and the remaining Ni were segregated again after Ni element was excluded by the (Ni, Sc)-rich phase with an FCC structure and ultimately formed a new phase with a BCC structure. However, the mixing enthalpy between Al and Sc (−38 kJ/mol) was slightly higher than that between Ni and Sc (−39 kJ/mol), which implied that a small amount of Sc segregation formed the BCC phase in addition to forming the FCC phase with Ni. The TEM analysis and the calculated mixing enthalpy indicated that during solidification, the (Co, Cr, Fe)-rich dendrite region with an FCC structure nucleated first from the liquid, and Al, Ni and Sc atoms were repelled from the dendritic region as the dendrite grew and

finally formed a (Ni, Sc)-rich interdendritic region with an FCC structure and an (Al, Ni)-rich interdendritic region with a BCC structure.

Table 3 Mixing enthalpies of atom-pairs between elements of $Al_{0.2}CoCrFeNiSc_x$ alloys [52] (kJ/mol)

Element	Element					
	Al	Co	Cr	Fe	Ni	Sc
Al	0	−19	−10	−11	−22	−38
Co	−19	0	−4	−1	0	−30
Cr	−10	−4	0	−1	−7	1
Fe	−11	−1	−1	0	−2	−11
Ni	−22	0	−7	−2	0	−39
Sc	−38	−30	1	−11	−39	0

4.2 Effect of Sc on hardness and mechanical properties

There are multiple contributions from solid solution strengthening, dislocation strengthening, precipitation strengthening, and grain size strengthening, etc, which increase the hardness and strength of HEA alloys. SRIHARITHA et al [53] reported that the hardness of $Al_xCoCrFeNi$ alloys increased with increasing the Al content, which was attributed to the grain size strengthening, solid solution strengthening, order strengthening and particles strengthening. The grain size strengthening and precipitation strengthening were the main strengthening mechanisms for $Al_{0.3}CoCrFeNi$ alloy [54]. The solid solution strengthening together with precipitation strengthening resulted in the increase of hardness for $Al_xCoCrFeNi$ alloys [3]. The improvement of strength for $AlCoCrFeNiSi_x$ alloys was attributed to the solid solution of Si element and precipitation strengthening of nanoscale cellular structure [22]. In the present study, solid solution strengthening, grain size strengthening and other strengthening factors from phase evolution are considered as the main strengthening mechanisms. The overall hardness of the alloy can be expressed as

$$HV_{total}=HV_{gss}+HV_{ss}+HV_0+HV_{oth} \quad (1)$$

where HV_{gss}, HV_{ss}, HV_0 and HV_{oth} represent the grain size hardening, solid solution hardening, lattice friction hardening and other hardening caused by phase evolution, respectively.

Since, HV_{gss} can be expressed as

$$HV_{gss}=K_{HV}d^{-1/2} \quad (2)$$

where K_{HV} is the Hall−Petch coefficient ($HV\cdot\mu m^{1/2}$) and d is the average grain size (μm). WU et al [55] reported that the CoCrFeNi alloy had a K_{HV} of 165.5 $HV\cdot\mu m^{1/2}$, while GWALANI et al [54] obtained a K_{HV} of 227.4 $HV\cdot\mu m^{1/2}$ for the $Al_{0.3}CoCrFeNi$ alloy. The addition of Al to CoCrFeNi alloy increased the value of Hall−Petch coefficient. Therefore, the value of K_{HV}= 227.4 $HV\cdot\mu m^{1/2}$ was used in the present study. The value of d is taken from Table 2. Taking the values of K_{HV} and d into Eq. (2), and the HV_{gss} was obtained. Since the HV_{gss} was calculated, the rest of contributions to hardness can be due to solid solution, lattice friction and other factor caused by the phase evolution. Different contributions are illustrated in Fig. 11(a).

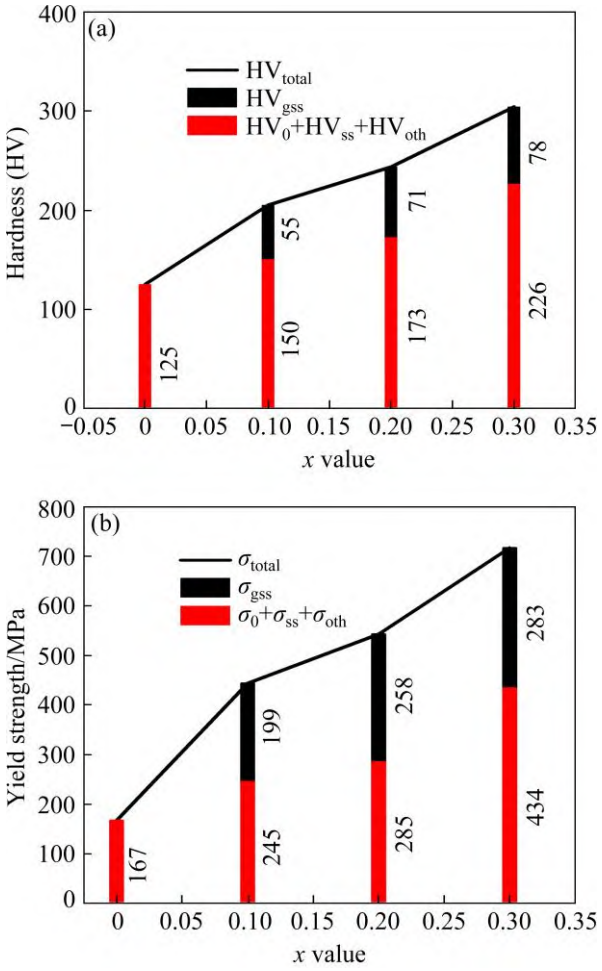

Fig. 11 Hardness (a) and yield strength (b) of $Al_{0.2}CoCrFeNiSc_x$ alloys as function of x value

Additionally, the effect of grain size on the yield strength was investigated. According to the Hall−Petch relationship, the yield strength caused by grain size strengthening (σ_{gss}) is given below:

$$\sigma_{gss}=K_{\sigma}d^{-1/2} \quad (3)$$

where K_{σ}(=824 MPa·μm$^{1/2}$) is a coefficient and taken from the literature [54].

The yield strength caused by solid solution, lattice friction and phase evolution can be expressed as

$$\sigma_{ss}+\sigma_0+\sigma_{oth}=\sigma_{total}-\sigma_{gss} \quad (4)$$

where σ_{ss}, σ_0 and σ_{oth} represent the solid solution strengthening, lattice friction strengthening and other strengthening caused by phase evolution, respectively.

Taking the values of K_{σ} and d into Eq. (3), the σ_{gss} was obtained. Similar to the contributions to hardness, different contributions to strength are illustrated in Fig. 11(b).

As seen from Fig. 11, the hardness increased from HV 55 to HV 78 and the yield strength increased from 199 to 283 MPa by Hall−Petch strengthening due to the decrease of grain size. It indicated that the grain refinement induced by the addition of Sc element played an important role in the improvement of mechanical properties for $Al_{0.2}$CoCrFeNi alloy. Additionally, the hardness and yield strength caused by solid solution, lattice friction and phase evolution increased with increasing the Sc content. The lattice friction was originated from the multicomponent characteristics of HEA alloys [56]. The values of HV_0 and σ_0 were determined as HV 125 and 167 MPa in accordance with the experimental hardness and yield strength in the $Al_{0.2}$CoCrFeNi alloy.

Solid solution strengthening is another main cause for improving the mechanical properties of HEA alloys [57]. TONG et al [3] believed that the increasing hardness with the increase of Al content in as-cast Al_xCoCrFeNi alloy was attributed to the solid solution hardening. SRIHARITHA et al [53] had drawn the same conclusion that the solid solution strengthening considerably increased with increasing Al content in sintered Al_xCoCrCuFeNi alloy. In recent years, some researcher have proposed physical models to describe solid solution strengthening of HEA alloys, such as Senkov model [58], Toda−Caraballo model [59] and Varvenne model [60], among which the Varvenne model successfully predicted the yield strength of Al_xCoCrFeNi and Al_xCoCrFeNiMn alloys [61]. According to the Varvenne model, the solid solution strengthening can be expressed as

$$\sigma_{ss}=0.01785M\alpha^{-1/3}G\left(\frac{1+v}{1-v}\right)^{4/3}\left[\frac{\sum_n(c_n\cdot\Delta V_n^2)}{b^6}\right]^{2/3} \quad (5)$$

where M is Taylor factor, α is dislocation line tensor parameter, G is shear modulus, v is Poisson ratio, b is the amplitude of Burgers vector, c_n is molar content of element n, and ΔV_n is misfit volume. $\sum_n(c_n\cdot\Delta V_n^2)$ can be expressed by the following equation [62]:

$$\sum_n(c_n\cdot\Delta V_n^2)=9V^2\left[\frac{\sum_n(c_n\cdot r_n^2)}{r^2}-1\right] \quad (6)$$

where V is the average atomic volume, r_n is the atomic radius of the element n, and r is the average atomic radius.

According to Eqs. (5) and (6), it can be inferred that the elements with large atomic radius added to HEA alloys could result in large misfit volume and thus enhance the strength of the alloy. The atomic radius of Sc is 2.09 Å, which is larger than that of Al (1.82 Å), Co (1.67 Å), Cr (1.88 Å), Fe (1.72 Å) and Ni (1.62 Å). Therefore, Sc element could cause solid solution strengthening. And with the increase of Sc content, the solid solution strengthening effect was improved. YIN et al [60] reported that V element with large atomic radius of 1.92 Å could induce large misfit volume and thus lead to high solid solution strengthening effect in Co−Cr−Fe−Mn−Ni−V and Cr−Mo−Nb−Ta−V−W−Hf−Ti−Zr alloy families.

In addition to grain size strengthening and solid solution strengthening, the phase evolution can also improve mechanical properties of the alloy. The hardness of Al_xCoCrFeNi alloys increased as the crystal structure changed from a single FCC phase to a mixed FCC+BCC phase [16,51]. In the present study, $Al_{0.2}$CoCrFeNi alloy was a single FCC phase, but it evolved into two types of FCC phases and one type of BCC phase after adding Sc. The volume fractions of (Co, Cr, Fe)-rich FCC phase, (Ni, Sc)-rich FCC phase and (Al, Ni)-rich BCC phase were calculated based on SEM images in order to better clarify the effects of different phases on the strength of the alloy, and the results are shown in Fig. 12. As seen from Fig. 12(a), the volume fraction of (Co, Cr, Fe)-rich FCC phase

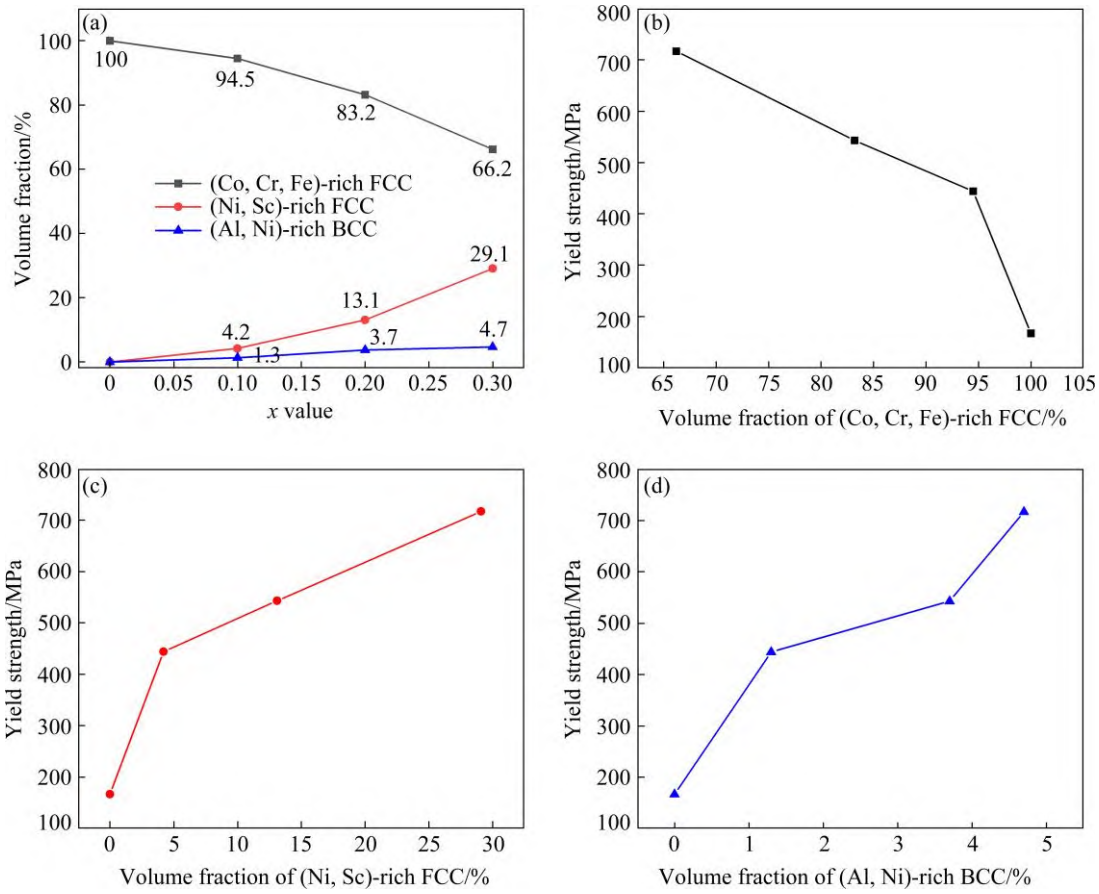

Fig. 12 Volume fractions of different phases with different Sc contents (a) and yield strength with volume fraction of different phases (b−d)

dramatically decreased, while the volume fractions of (Ni, Sc)-rich FCC phase and (Al, Ni)-rich BCC phase increased as the Sc content increased. The yield strength decreased with increasing the volume fraction of (Co, Cr, Fe)-rich FCC phase, but increased with increasing the volume fraction of (Ni, Sc)-rich FCC phase and (Al, Ni)-rich BCC phase, as shown in Figs. 12(b−d). Therefore, it can be concluded that the formation of (Ni, Sc)-rich FCC phase and (Al, Ni)-rich BCC phase played an important role in improving the yield strength of the alloy.

5 Conclusions

(1) Sc had an apparent grain-refining effect on the $Al_{0.2}CoCrFeNiSc_x$ alloys. As the Sc content increased, the grain size decreased. The grain size of $Al_{0.2}CoCrFeNiSc_{0.3}$ alloy (8.5 μm) was reduced by approximately 50.6% compared to that of $Al_{0.2}CoCrFeNiSc_{0.1}$ alloy (17.2 μm).

(2) The phase evolved from a single FCC phase to a mixed phase, including two types of FCC phases and one type of BCC phase. The FCC phase appeared in the regions of (Co, Cr, Fe)-rich dendrites and (Ni, Sc)-rich interdendrites, while the BCC phase was mainly located in the region of (Al, Ni)-rich interdendrites. Sc tended to segregate at the interdendrite and formed FCC structure.

(3) Sc effectively improved the mechanical properties of $Al_{0.2}CoCrFeNiSc_x$ alloys. The hardness increased from HV 125 to HV 304 and the yield strength increased from 167 to 717 MPa as the Sc content increased from 0 to 0.3. The hardness was improved by 143.2% and the yield strength was improved by 329.3%.

(4) Grain size strengthening, solid solution strengthening and phase evolution were responsible for the improvement of yield strength. The addition of Sc reduced the grain size and increased the misfit volume, thereby inducing grain size strengthening and solid solution strengthening. The formation of (Ni, Sc)-rich FCC phase and (Al, Ni)-rich BCC phase also improved the yield strength.

Acknowledgments

The work was supported by the Natural Science Foundation of Shandong Province, China (No. ZR2021QE136).

References

[1] LI Wei-dong, XIE Di, LI Dong-yue, ZHANG Yong, GAO Yan-fei, LIAW P K. Mechanical behavior of high-entropy alloys [J]. Progress in Materials Science, 2021, 118: 100777.

[2] ZHOU Y J, ZHANG Y, WANG Y L, CHEN G L. Solid solution alloys of AlCoCrFeNiTi$_x$ with excellent room-temperature mechanical properties [J]. Applied Physics Letters, 2007, 90: 181904.

[3] TONG C J, CHEN M R, YEH J W, CHEN S K, SHUN T T, LIN S J, CHANG S Y. Mechanical performance of the Al$_x$CoCrCuFeNi high-entropy alloy system with multiprincipal elements [J]. Metallurgical and Materials Transactions A, 2005, 36(5): 1263−1271.

[4] LI Dong-yue, ZHANG Yong. The ultrahigh Charpy impact toughness of forged Al$_x$CoCrFeNi high entropy alloys at room and cryogenic temperatures [J]. Intermetallics, 2016, 70: 24−28.

[5] CHAUDHARY V, CHAUDHARY R, BANERJEE R, RAMANUJAN R V. Accelerated and conventional development of magnetic high entropy alloys [J]. Materials Today, 2021, 49: 231−252.

[6] HUO Wen-yi, WANG Shi-qi, ZHU Wen-han, ZHANG Ze-ling, FANG Feng, XIE Zong-han, JIANG Jian-qing. Recent progress on high-entropy materials for electro-catalytic water splitting applications [J]. Tungsten, 2021, 3(2): 161−180.

[7] YANG Yu, LUO Xiang-yu, MA Tong-xiang, WEN Liang-ying, HU Li-wen, HU Mei-long. Effect of Al on characterization and properties of Al$_x$CoCrFeNi high entropy alloy prepared via electro-deoxidization of the metal oxides and vacuum hot pressing sintering process [J]. Journal of Alloys and Compounds, 2021, 864: 158717.

[8] KAO Y F, CHEN S K, CHEN T J, CHU P C, YEH J W, LIN S J. Electrical, magnetic, and Hall properties of Al$_x$CoCrFeNi high-entropy alloys [J]. Journal of Alloys and Compounds, 2011, 509(5): 1607−1614.

[9] WANG Nai-ran, WANG Shou-ren, GOU Xiao-xiang, SHI Ze-cheng, LIN Jian-xiang, LIU Guo-qiang, WANG Yan. Alloying behavior and characterization of (CoCrFeNiMn)$_{90}$-M$_{10}$ (M=Al, Hf) high-entropy materials fabricated by mechanical alloying [J]. Transactions of Nonferrous Metals Society of China, 2022, 32(7): 2253−2265.

[10] DU Hui, CAI Jia-hong, WANG Ya-song, YAO Jun-qing, CHEN Qiang, CUI Yu, LIU Xin-wang. Effect of partial recrystallization on microstructure and tensile properties of NiFeCoCrMn high-entropy alloy [J]. Transactions of Nonferrous Metals Society of China, 2022, 32(3): 947−956.

[11] ZHUANG Y X, XUE H D, CHEN Z Y, HU Z Y, HE J C. Effect of annealing treatment on microstructures and mechanical properties of FeCoNiCuAl high entropy alloys [J]. Materials Science and Engineering A, 2013, 572: 30−35.

[12] OH M C, SHARMA A, LEE H, AHN B. Phase separation and mechanical behavior of AlCoCrFeNi−X (X=Cu, Mn, Ti) high entropy alloys processed via powder metallurgy [J]. Intermetallics, 2021, 139: 107369.

[13] CHENG Q, XU X D, XIE P, HAN L L, HE J Y, LI X Q, ZHANG J, LI Z T, LI Y P, LIU B, NIEH T G, CHEN M W, CHEN J H. Unveiling anneal hardening in dilute Al-doped Al$_x$CoCrFeMnNi (x= 0, 0.1) high-entropy alloys [J]. Journal of Materials Science & Technology, 2021, 91: 270−277.

[14] XU Jun, CAO Cheng-ming, GU Ping, PENG Liang-ming. Microstructures, tensile properties and serrated flow of Al$_x$CrMnFeCoNi high entropy alloys [J]. Transactions of Nonferrous Metals Society of China, 2020, 30(3): 746−755.

[15] WANG W R, WANG W L, YEH J W. Phases, microstructure and mechanical properties of Al$_x$CoCrFeNi high-entropy alloys at elevated temperatures [J]. Journal of Alloys and Compounds, 2014, 589: 143−152.

[16] WANG W R, WANG W L, WANG S C, TSAI Y C, LAI C H, YEH J W. Effects of Al addition on the microstructure and mechanical property of Al$_x$CoCrFeNi high-entropy alloys [J]. Intermetallics, 2012, 26: 44−51.

[17] TUNG C C, YEH J W, SHUN T T, CHEN S K, HUANG Y S, CHEN H C. On the elemental effect of AlCoCrCuFeNi high-entropy alloy system [J]. Materials Letters, 2007, 61(1): 1−5.

[18] WANG X F, ZHANG Y, QIAO Y, CHEN G L. Novel microstructure and properties of multicomponent CoCrCuFeNiTi$_x$ alloys [J]. Intermetallics, 2007, 15(3): 357−362.

[19] CHEN M R, LIN S J, YEH J W, CHEN W K, HUANG Y S, CHUANG M H. Effect of vanadium addition on the microstructure, hardness, and wear resistance of Al$_{0.5}$CoCrCuFeNi high-entropy alloy [J]. Metallurgical and Materials Transactions A, 2006, 37(5): 1363−1369.

[20] ZHANG Ji-feng, ZHU He-guo, XIE Zong-han. Effects of Y and Al additions on the microstructure and tensile properties of CoCr$_3$Fe$_5$Ni high entropy alloys [J]. Materials Letters, 2021, 299: 130110.

[21] MA S G, ZHANG Y. Effect of Nb addition on the microstructure and properties of AlCoCrFeNi high-entropy alloy [J]. Materials Science and Engineering A, 2012, 532: 480−486.

[22] ZHU J M, FU H M, ZHANG H F, WANG A M, LI H, HU Z Q. Synthesis and properties of multiprincipal component AlCoCrFeNiSi$_x$ alloys [J]. Materials Science and Engineering A, 2010, 527(27): 7210−7214.

[23] HSU C Y, YEH J W, CHEN S K, SHUN T T. Wear resistance and high-temperature compression strength of Fcc CuCoNiCrAl$_{0.5}$Fe alloy with boron addition [J]. Metallurgical and Materials Transactions A, 2004, 35(5): 1465−1469.

[24] QIN Jin, TAN Pan, QUAN Xiang, LIU Zheng-qing, YI Dan-qing, WANG Bin. The effect of sc addition on microstructure and mechanical properties of as-cast Zr-containing Al−Cu alloys [J]. Journal of Alloys and Compounds, 2022, 909: 164686.

[25] COSTA S, PUGA H, BARBOSA J, PINTO A M P. The effect of Sc additions on the microstructure and age hardening behaviour of as cast Al−Sc alloys [J]. Materials & Design, 2012, 42: 347−352.

[26] MA Juan, YAN De-sheng, RONG Li-jian, LI Yi-yi. Effect of Sc addition on microstructure and mechanical properties of 1460 alloy [J]. Progress in Natural Science: Materials International, 2014, 24(1): 13−18.

[27] SUN Yu-qiao, LUO Yu-hong, PAN Qing-lin, LIU Bing, LONG Liang, WANG Wei-yi, YE Ji, HUANG Zhi-qi, XIANG Sheng-qian. Effect of Sc content on microstructure and properties of Al−Zn−Mg−Cu−Zr alloy [J]. Materials Today Communications, 2021, 26: 101899.

[28] HUANG Xing, PAN Qing-lin, LI Bo, LIU Zhi-ming, HUANG Zhi-qi, YIN Zhi-min. Microstructure, mechanical properties and stress corrosion cracking of Al−Zn−Mg−Zr alloy sheet with trace amount of Sc [J]. Journal of Alloys and Compounds, 2015, 650: 805−820.

[29] WANG Kai-xian, YIN Deng-feng, ZHAO Ying-chao, ATRENS A, ZHAO Ming-chun. Microstructural evolution upon heat treatments and its effect on corrosion in Al−Zn−Mg alloys containing Sc and Zr [J]. Journal of Materials Research and Technology, 2020, 9(3): 5077−5089.

[30] DENG Ying, PENG Bing, XU Guo-fu, PAN Qing-lin, YE Rui, WANG Ying-jun, LU Li-ying, YIN Zhi-min. Stress corrosion cracking of a high-strength friction-stir-welded joint of an Al−Zn−Mg−Zr alloy containing 0.25 wt.% Sc [J]. Corrosion Science, 2015, 100: 57−72.

[31] KNIPLING K E, SEIDMAN D N, DUNAND D C. Ambient- and high-temperature mechanical properties of isochronally aged Al−0.06Sc, Al−0.06Zr and Al−0.06Sc−0.06Zr (at.%) alloys [J]. Acta Materialia, 2011, 59(3): 943−954.

[32] YIN Song-bo, HUANG Bo-yun, YIN Zhi-min. Effect of minor Sc on high temperature mechanical properties of Ti−Al based alloys [J]. Materials Science and Engineering A, 2000, 280(1): 204−207.

[33] LIU H Q, YI D Q, ZHENG F. The influence of Sc on α/β transformation of Ti [J]. Materials Science and Engineering A, 2008, 487(1): 58−63.

[34] LÜ Yi-zhen, WANG Qu-dong, ZENG Xiao-qin, DING Wen-jiang, ZHAI Chun-quan, ZHU Yan-ping. Effects of rare earths on the microstructure, properties and fracture behavior of Mg−Al alloys [J]. Materials Science and Engineering A, 2000, 278(1): 66−76.

[35] SVISTUNOVA T V, BOBKOVA O S, BELYASOV B D. Effect of scandium on structure and properties of corrosion-resistant steels [J]. Metal Science and Heat Treatment, 2008, 50(5): 214−219.

[36] RIVA S, MEHRABAN S, LAVERY N P, SCHWARZMÜLLER S, OECKLER O, BROWN S G R, YUSENKO K V. The effect of scandium ternary intergrain precipitates in Al-containing high-entropy alloys [J]. Entropy, 2018, 20(7): 488.

[37] YUSENKO K V, RIVA S, CRICHTON W A, SPEKTOR K, BYKOVA E, PAKHOMOVA A, TUDBALL A, KUPENKO I, ROHRBACH A, KLEMME S, MAZZALI F, MARGADONNA S, LAVERY N P, BROWN S G R. High- pressure high-temperature tailoring of high entropy alloys for extreme environments [J]. Journal of Alloys and Compounds, 2018, 738: 491−500.

[38] RIVA S, FUNG C M, SEARLE J R, CLARK R N, LAVERY N P, BROWN S G R, YUSENKO K V. Formation and disruption of W-phase in high-entropy alloys [J]. Metals, 2016, 6(5): 106.

[39] YOUSSEF K M, ZADDACH A J, NIU C N, IRVING D L, KOCH C C. A novel low-density, high-hardness, high-entropy alloy with close-packed single-phase nanocrystalline structures [J]. Materials Research Letters, 2015, 3(2): 95−99.

[40] RIVA S, BROWN S G R, LAVERY N P, YUSENKO K V. Scandium-based hexagonal-closed packed multi-component alloys [J]. Physics of Metals and Metallography, 2018, 119(8): 735−740.

[41] TAKEUCHI A, AMIYA K, WADA T, YUBUTA K. Dual HCP structures formed in senary ScYLaTiZrHf multi-principal-element alloy [J]. Intermetallics, 2016, 69: 103−109.

[42] KRNEL M, JELEN A, VRTNIK S, LUZAR J, GAČNIK D, KOŽELJ P, WENCKA M, MEDEN A, HU Q, GUO S, DOLINŠEK J. The effect of scandium on the structure, microstructure and superconductivity of equimolar Sc−Hf−Nb−Ta−Ti−Zr refractory high-entropy alloys [J]. Materials, 2022, 15(3): 1122.

[43] TAKEUCHI A, INOUE A. Classification of bulk metallic glasses by atomic size difference, heat of mixing and period of constituent elements and its application to characterization of the main alloying element [J]. Materials Transactions, 2005, 46(12): 2817−2829.

[44] RUAN Y, MOHAJERANI A, DAO M. Microstructural and mechanical-property manipulation through rapid dendrite growth and undercooling in an Fe-based multinary alloy [J]. Scientific Reports, 2016, 6: 31684.

[45] CAO Zhao-ping, LIU Shu-hong, FANG Xu, CHENG Kai-ming, GAO Qian-nan, DU Yong, WANG Jiong, ZHANG Jun, HUANG Wei-dong, TANG Cheng-ying. Experimental investigation and thermodynamic analysis of the Sc−Ni system supplemented with first-principles calculations [J]. Thermochimica Acta, 2014, 586: 30−39.

[46] KARDELLASS S, SERVANT C, SELHAOUI N, IDDAOUDI A, AMAR M A, BOUIRDEN L. Thermodynamic description of the Ni−Sc system [J]. Calphad, 2013, 42: 59−65.

[47] MOUSAVI M G, CROSS C E, GRONG Ø. Effect of scandium and titanium−boron on grain refinement and hot cracking of aluminium alloy 7108 [J]. Science and Technology of Welding and Joining, 1999, 4(6): 381−388.

[48] COSTELLO F A, ROBSON J D, PRANGNELL P B. The effect of small scandium additions to AA7050 on the as-cast and homogenized microstructure [J]. Materials Science Forum, 2002, 396: 757−762.

[49] YANG Teng-fei, XIA Song-qin, LIU Shi, WANG Chen-xu, LIU Shao-shuai, ZHANG Yong, XUE Jian-ming, YAN Sha, WANG Yu-gang. Effects of Al addition on microstructure and mechanical properties of $Al_xCoCrFeNi$ High-entropy alloy [J]. Materials Science and Engineering A, 2015, 648: 15−22.

[50] MA S G, LIAW P K, GAO M C, QIAO J W, WANG Z H, ZHANG Y. Damping behavior of $Al_xCoCrFeNi$ high-entropy alloys by a dynamic mechanical analyzer [J]. Journal of Alloys and Compounds, 2014, 604: 331−339.

[51] KAO Y F, CHEN T J, CHEN S K, YEH J W. Microstructure and mechanical property of as-cast, homogenized, and deformed $Al_xCoCrFeNi$ ($0 \le x \le 2$) high-entropy alloys [J].

Journal of Alloys and Compounds, 2009, 488(1): 57−64.
[52] BOER F R D, BOOM R, MATTENS W C M, MIEDEMA A R, NIESSEN A K. Cohesion in metals: Transition metal alloys [M]. Amsterdam: Elesvier, 1989.
[53] SRIHARITHA R, MURTY B S, KOTTADA R S. Alloying, thermal stability and strengthening in spark plasma sintered $Al_xCoCrCuFeNi$ high entropy alloys [J]. Journal of Alloys and Compounds, 2014, 583: 419−426.
[54] GWALANI B, SONI V, LEE M, MANTRI S A, REN Y, BANERJEE R. Optimizing the coupled effects of Hall−Petch and precipitation strengthening in a $Al_{0.3}CoCrFeNi$ high entropy alloy [J]. Materials & Design, 2017, 121: 254−260.
[55] WU Z, BEI H, OTTO F, PHARR G M, GEORGE E P. Recovery, recrystallization, grain growth and phase stability of a family of FCC-structured multi-component equiatomic solid solution alloys [J]. Intermetallics, 2014, 46: 131−140.
[56] YOSHIDA S, BHATTACHARJEE T, BAI Y, TSUJI N. Friction stress and Hall−Petch relationship in CoCrNi equi-atomic medium entropy alloy processed by severe plastic deformation and subsequent annealing [J]. Scripta Materialia, 2017, 134: 33−36.
[57] CARABALLO I T, RIVERA P E J. Modelling solid solution hardening in high entropy alloys [J]. Acta Materialia, 2015, 85: 14−23.
[58] COURY F G, KAUFMAN M, CLARKE A J. Solid−solution strengthening in refractory high entropy alloys [J]. Acta Materialia, 2019, 175: 66−81.
[59] MENOU E, CARABALLO I T, RIVERA P E J, PINEAU C, BERTRAND E, RAMSTEIN G, TANCRET F. Evolutionary design of strong and stable high entropy alloys using multi-objective optimisation based on physical models, statistics and thermodynamics [J]. Materials & Design, 2018, 143: 185−195.
[60] YIN Bing-lun, MARESCA F, CURTIN W A. Vanadium is an optimal element for strengthening in both fcc and bcc high-entropy alloys [J]. Acta Materialia, 2020, 188: 486−491.
[61] VARVENNE C, CURTIN W A. Strengthening of high entropy alloys by dilute solute additions: $CoCrFeNiAl_x$ and $CoCrFeNiMnAl_x$ alloys [J]. Scripta Materialia, 2017, 138: 92−95.
[62] VARVENNE C, LUQUE A, CURTIN W A. Theory of strengthening in fcc high entropy alloys [J]. Acta Materialia, 2016, 118: 164−176.

Sc 添加对 $Al_{0.2}CoCrFeNi$ 高熵合金显微组织、相演变及力学性能的影响

孙元伟[1]，王子懿[1]，赵相金[1]，刘仲礼[1]，曹富华[2]

1. 烟台大学 核装备与核工程学院，烟台 264005；
2. 中国科学院 力学研究所，北京 100190

摘　要：采用电弧熔炼法制备 $Al_{0.2}CoCrFeNiSc_x$ (x=0, 0.1, 0.2, 0.3, 摩尔分数)合金，研究 Sc 添加对合金显微组织、相演变和力学性能的影响。结果表明，Sc 能细化晶粒、改变相类型以及提高合金的力学性能。相较于 $Al_{0.2}CoCrFeNiSc_{0.1}$ 合金的晶粒尺寸(17.2 μm)，$Al_{0.2}CoCrFeNiSc_{0.3}$ 合金的晶粒尺寸仅为 8.5 μm，减小了约 50.6%。合金的晶体结构由 FCC 相演变为包括两种 FCC 相和一种 BCC 相的混合相。FCC 相主要出现在富 Co、Cr 和 Fe 枝晶区域和富 Ni 和 Sc 枝晶间区域，而 BCC 相主要出现在富 Al 和 Ni 枝晶间区域。当 $Al_{0.2}CoCrFeNiSc_x$ 合金中 x 值由 0 增加到 0.3 时，合金的屈服强度由 167 MPa 增加至 717 MPa，提高了 329.3%，这主要归因于晶粒强化、固溶强化和相演变。

关键词：高熵合金；相演变；显微组织；晶粒细化；屈服强度

(Edited by Wei-ping CHEN)